Corrosion Science 80 (2014) 269–275

Contents lists available at ScienceDirect

Corrosion Science

journal homepage: www.elsevier.com/locate/corsci

Polybenzoxazine/SiO_2 nanocomposite coatings for corrosion protection of mild steel

Changlu Zhou [a], Xin Lu [a], Zhong Xin [a,*], Juan Liu [a], Yanfeng Zhang [b]

[a] State Key Laboratory of Chemistry Engineering, School of Chemical Engineering, East China University of Science and Technology, Shanghai 200237, China
[b] Lanpec Technologies Co, Ltd., Gansu 730070, China

ARTICLE INFO

Article history:
Received 18 April 2013
Accepted 26 November 2013
Available online 4 December 2013

Keywords:
A. Mild steel
B. EIS
B. IR spectroscopy
B. SEM
C. Polymer coatings

ABSTRACT

A series of nanocomposite coatings (PBS) consisting of silane functional polybenzoxazine (PB-TMOS) and SiO_2 nanoparticles were developed for corrosion protection of mild steel. The influence of silica content on corrosion resistance of PBS coatings was investigated by electrochemical measurements. The surface chemistry of nanoparticles and its effect on morphology of the PBS coating was also studied utilizing Fourier Transforms Infrared Spectroscopy, ^{29}Si Nuclear Magnetic Resonance and Scanning Electron Microscopy analyses. The results indicate that the presence of the covalent bond between nanoparticles and PB-TMOS, greatly improves the interfacial interactions at the polymer/filler interfaces resulting in a better corrosion performance.

1. Introduction

In the past decade, nanometer size fillers have been considered playing an important role in the improvement of corrosion resistance, thermal and mechanical properties of the coatings [1–3]. Organic coatings have been employed to protect steel surfaces against versatile corrosion environments for a long time by introducing a barrier to prevent ionic transport and electrical conduction [4,5]. There are various reports concerning improving coatings' performance in such environments using nanoparticles as reinforcements such as, TiO_2 [6,7], SiO_2 [8], ZnO [9,10], ZrO_2 [11], and Fe_2O_3 [12].

SiO_2 is one of the most promising nanoparticles employed in corrosion protection coatings. They have many excellent properties such as high hardness (7 Mohs), low refractive index (1.46), and reasonable price among other nanoparticles which make it ideal to produce scratch-resistant, transparent and cost-effective coatings and high absorption of ultra violet (UV) radiation [13,14]. However, it should also be noted that the surface of the silica nanoparticles contains OH functionalities causing inherent hydrophilicity to these particles. Phase separation might occur due to the incompatibility of hydrophilic silica nanoparticles with non-polar or weakly polar matrices, which inhibit SiO_2 nanoparticles' use as good filler for corrosion protection coatings.

Recently, polybenzoxazines have the potential to apply as corrosion protective coating due to their unique properties such as low water absorption [15], low surface free energy [16,17], near-zero shrinkage [18], and excellent dielectric properties [19,20], which are superior to those of epoxy resins and conventional phenolics. In our previous studies, we have synthesized a novel silane-functional polybenzoxazine precursor (B-TMOS) and prepared its polymeric coating (PB-TMOS) via dip coating and traditional thermal curing method, which revealed good corrosion protection for steels [21]. A mechanism for enhanced corrosion resistance of PB-TMOS coating has been suggested to include the dual cross-linking network of polybenzoxazine and Si–O–Si in the PB-TMOS matrix and its strong hydrophobic property and substrate adhesion. Furthermore, active alkoxy groups of B-TMOS could hydrolyze during the dip coating process and convert to silanols (SiOH), which will easily react with the hydroxyl groups on the surface of SiO_2 nanoparticles through covalent bond [22]. It can make SiO_2 nanoparticles tightly bound to the PB-TMOS matrix without any incompatibility problems.

Therefore, SiO_2 nanoparticle has been incorporated into PB-TMOS coating in order to improve the PB-TMOS/SiO_2 nanocomposite (PBS) coating's corrosion resistance in this study. We present the first preparation of PBS coating only by physical blending without any other treatment. Cross-linking interaction between B-TMOS monomer and SiO_2 nanoparticles is characterized by Fourier Transforms Infrared (FTIR) spectroscopy, and ^{29}Si Nuclear Magnetic Resonance (NMR) spectroscopy. Effects of SiO_2 nanoparticles content in the PBS coating on the wettability, surface morphology

* Corresponding author. Tel.: +86 21 64240862; fax: +86 21 64251772.
E-mail address: xzh@ecust.edu.cn (Z. Xin).

0010-938X/$ - see front matter © 2013 Elsevier Ltd. All rights reserved.
http://dx.doi.org/10.1016/j.corsci.2013.11.042

and corrosion protection ability for MS have been investigated by water contact angle, Scanning Electron Microscopy (SEM) and electrochemical measurements in 3.5 wt% NaCl aqueous solutions, respectively.

2. Experimental

2.1. Materials and chemical reagents

The mild steel (MS) (Q235B, composition in wt%: C: 0.12, Mn: 0.32, Cr: 0.035, Si: 0.14, Ni: 0.040, S: 0.010, P: 0.012, Cu: 0.010, Fe: balance) was provided by Lanpec Technologies Co. Ltd, China. Bisphenol A was purchased from Sinopharm Chemical Reagent Co. Ltd, China. 3-Aminopropyltrimethoxysilane (3-APTMOS) was obtained from Diamond Advanced Material of Chemical Inc., China. SiO_2 nanoparticles with a mean diameter of 15–20 nm and a specific area of 200 $m^2\ g^{-1}$, was provided by Prof. Li's group [23]. Paraformaldehyde, chloroform, xylene, *n*-butanol and other chemicals were from Shanghai Lingfeng Chemical Corp., China. All chemicals were of analytical pure reagent grade. Chloroform was purified by distillation over calcium hydride (CaH_2) prior to use; all other chemicals were used as received.

2.2. Synthesis of benzoxazine monomer

2,2-Bis(3-(trimethoxysilyl)-n-propyl-3,4-dihydro-2H-1,3-benzoxazine)-propane (B-TMOS) was synthesized by a method available in the literature (Fig. 1) [17]. The product was yellow liquid with a yield of 85.1%. FTIR (KBr): v = 1498 (tri-substituted phenyl group); 1231 (s; v_{as} (C–O–C of benzoxazine ring)), 1016 (s; v_s (C–O–C of benzoxazine ring)); 1085 (s; v_{as} (Si–O–C)); 931 (oxazine ring). ^{1}H NMR (400 MHz, chloroform-d, δ): 6.75–7.26 (m, 6H, ArH), 4.82 (s, 4H, O–CH_2–N), 3.98 (s, 4H, Ph–CH_2–N), 3.58 (s, 18H, Si–O–CH_3), 2.73 (t, 4H, N–CH_2), 1.66 (m, 4H, –CH_2–CH_2Si), 0.67 (t, 4H, –CH_2–Si).

2.3. Preparation of PB-TMOS/SiO_2 nanocomposite coatings

Bare MS was used as substrates. The substrates were blasted to Sa 2½, and then degreased with acetone. The designated amounts of SiO_2 nanoparticles of 0, 1, 3, and 5 wt% and B-TMOS monomer were dispersed into the mixed solvent (xylene/*n*-butanol = 7:3) at 180 mg ml^{-1} in an ultrasonic bath until uniform and transparent solutions were obtained. MS plates were dip coated into the B-TMOS or B-TMOS/SiO_2 solution for six times with a withdraw speed of 320 mm min^{-1}. There was no waiting time between consecutive immersion steps. The substrates remained in the solution for 1 min every time. Then, the residual solvent was removed by drying in vacuum at 100 °C for 1 h. Finally, the coated samples were cured in one step at 230 °C for 2 h. Samples obtained by mixing 0, 1, 3, and 5 wt% SiO_2 nanoparticles with B-TMOS were labeled by PB-TMOS, PBS1, PBS3, and PBS5, respectively. The thickness of the coatings was evaluated on the stainless steel surfaces before and after coating using a micrometer (Mitutoyo, Japan), resulting on thicknesses of ~5 μm for all coatings.

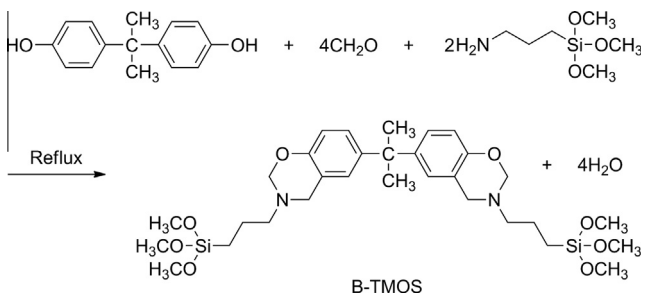

Fig. 1. Synthesis route of B-TMOS.

2.4. Characterization

2.4.1. Surface properties

Surface morphology of the coated MS was characterized by Scanning Electron Microscopy (Nova SEM 450, FEI). Static contact angles of the samples were determined by contact angle goniometry at 25 °C using a DataPhysicsOCA20 optical goniometer interfaced with image-capture software by injecting a 2 μL liquid drop. Deionized water was used as the test liquid. In order to obtain reliable contact angle data, five droplets were dispensed at different regions of the films. Atomic force microscopy (AFM) results were acquired using a Digital Instruments multimode scanning probe microscope (NanoScope IIIa). Damage to both the tip and the sample surface was minimized by employing AFM in tapping mode. The rms roughnesses were calculated over scanned area of 20 μm × 20 μm.

2.4.2. Fourier Transforms Infrared (FTIR) spectroscopy

FTIR measurements were carried out on a Nicolet iS10 FTIR spectrometer at room temperature (~25 °C) using the KBr pellet method. In all cases, 32 scans at a resolution of 1 cm^{-1} were recorded.

2.4.3. Nuclear Magnetic Resonance (NMR) spectroscopy

NMR spectra were measured at room temperature on a Bruker Avance 500 MHz spectrometer equipped with a Bruker solid-state accessory.

2.4.4. Corrosion evaluations

Electrochemical measurements were measured with a CH Instruments CHI660D (USA) workstation with a three-electrode system. The coated sample acted as the working electrode, a Ag/AgCl (saturated KCl) electrode was used as the reference electrode, and a stainless steel cylinder as the counter electrode. The electrode working area was ~14 cm^2. Electrochemical corrosion measurements were investigated using a potentiodynamic polarization technique, open circuit potential (E_{ocp})–time curves and electrochemical impedance spectroscopy (EIS). All tests were performed in a corrosive medium (3.5 wt% NaCl aqueous solutions) at ambient temperature. Samples were immersed for 30 min to ensure the steady-state prior to measurements; measurements were repeated at least three times. In the polarization current experiments, the potential was scanned from −100 mV below to +100 mV (Ag/AgCl) above the corrosion potential E_{corr} at a scan rate of 2 mV s^{-1}. The corrosion current I_{corr} and E_{corr} were obtained automatically from the Tafel plots using the CHI660D workstation analysis software. In the electrochemical impedance spectroscopy (EIS) measurements, a sinusoidal AC perturbation of 10 mV amplitude coupled with the open circuit potential was applied to the metal/coating system. The EIS test was managed in the frequency range from 100 kHz to 0.01 Hz. EIS analysis was performed by using Zview software.

3. Results and discussion

3.1. Surface modification of PBS coating with SiO_2 nanoparticles

Typical top-view SEM micrographs of PB-TMOS/SiO_2 nanocomposite coatings with various ratios of SiO_2 nanoparticles are displayed in Fig. 1. It was evident that the cured neat PB-TMOS coating was uniform, smooth without cracks (Fig. 2a). However,

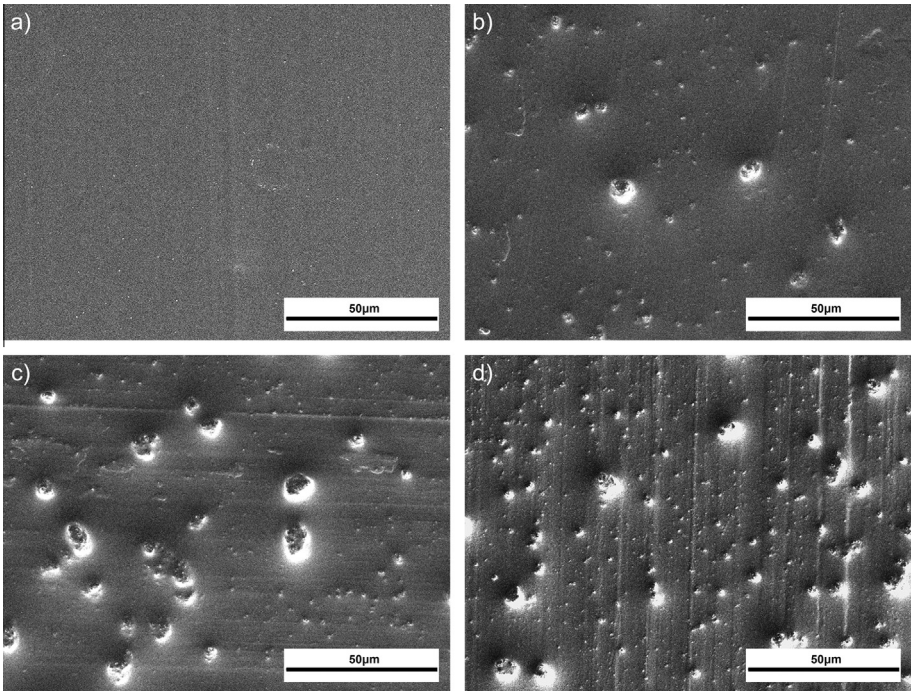

Fig. 2. Scanning electron micrographs of composite coatings containing (a) 0 wt%, (b) 1 wt%, (c) 3 wt%, (d) 5 wt% SiO_2 nanoparticles.

the surface morphology of the coatings was remarkably changed when they are modified with different amount of SiO_2 nanoparticles. Some aggregates could be clearly observed in the PBS samples, and from these graphs, it was suggested that the amount of aggregates increased with increasing nanoparticles content. That is because materials exhibit high surface free energy due to effects resulting from a high surface area to volume ratios at nanometer length scales. Especially in our system, the SiO_2 nanoparticles were incorporated without surface modification in order to guarantee the reaction between hydroxyl groups on the surface of nanoparticles and B-TMOS monomer. Aggregation would occur ascribed to the direct mutual attraction between particles via van der Waals forces or hydrogen bonding. With increasing the content of silica nanoparticles, more nanoparticles would participate in the interaction between nanoparticles. This was the reason why the amount of aggregates increased with the increase in the SiO_2 nanoparticles content from Fig. 2a–d. But based on the SEM results the question arises: why did the particles in nanometer form aggregates in micrometer? It must be related to the interactions between PB-TMOS and silica nanoparticles, which would be investigated in detail utilizing FTIR and solid-state ^{29}Si NMR spectroscopy below.

Contact angle (CA) measurements were taken for bare MS and various coated samples in order to investigate the surface hydrophobicity, shown in Table 1. It was seen that MS samples become more hydrophobic after coated with PB-TMOS or PBS coatings. The CAs of all coated MS were more than 100°, which were much higher than bare MS (75.0 ± 0.7°). It was also observed that CAs of coated samples increased slightly with increasing SiO_2 nanoparticles content. That is because the surface of PBS coatings was roughed by incorporating SiO_2 nanoparticles, which was verified by AFM results in Table 1. According to the Wenzel hypothesis [24], increasing the roughness of a hydrophobic surface increases its hydrophobicity. Wang et al. [25] even fabricated a superhydrophobic film based on polybenzoxazine by increasing the roughness of the coating with SiO_2 nanoparticles. But to avoid reducing the adhesion of PBS coating on the substrates, the addition of nanoparticles in our system (<5 wt%) was much lower than Wang's report (40–50 wt%). Therefore, it was obtained only a slight improvement on hydrophobicity of PB-TMOS/SiO_2 nanocomposite coating by incorporating SiO_2 nanoparticles. The hydrophobic nature of nanocomposite coatings also showed that SiO_2 nanoparticles and aggregates were totally embedded in the PB-TMOS matrix without exposure to the surface. This increased hydrophobicity might decrease the wettability of aggressive electrolytes, which could be limited on the coating surface. The barrier for corrosion under prolonged contact with aggressive media would be improved due to a very low portion of the coating area was in real contact with electrolyte solution [26,27]. It must be beneficial for their better corrosion resistance in wet environments.

Table 1
Surface roughness and contact angles (water) on bare MS and coated MS samples.

Samples	Rms roughness (nm)	Contact angle (°)
MS	–	75.0 ± 0.7
PB-TMOS	6.8	104.2 ± 0.3
PBS1	10.0	104.3 ± 0.3
PBS3	23.4	105.2 ± 0.4
PBS5	26.5	105.3 ± 0.3

3.2. Cross-linking interactions between PB-TMOS and SiO_2 nanoparticles in the PBS coatings

In order to investigate the cross-linking reaction, the SiO_2 nanoparticles in a mixture of B-TMOS and 3 wt% SiO_2 nanoparticles was separated by the operation cycle of centrifugal separation and washing with tetrahydrofuran (THF), and dried at 60 °C in vacuum for 48 h consequently. The term "separated SiO_2 nanoparticles" was referred to these treated nanoparticles. Fig. 3 shows the representative FTIR absorption spectra of the B-TMOS monomer, neat and separated SiO_2 nanoparticles. The absorption peak corresponding to asymmetric stretching of C–O–C (1233 cm^{-1}) [28,29], out plane bending vibrations of C–H of oxazine ring (928 cm^{-1}) [30] and trisubstituted benzene (1500 cm^{-1}) [31], were assigned to

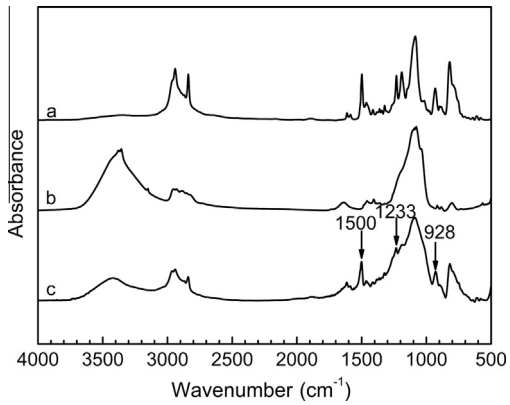

Fig. 3. FTIR spectra of (a) B-TMOS monomer, (b) neat and (c) separated SiO_2 nanoparticle.

the existence of the oxazine ring, appeared at the FTIR curve of separated SiO_2 nanoparticle in Fig. 3. Since B-TMOS monomer or oligomer should be washed by THF, the results of FTIR indicated that B-TMOS monomer had been coupled onto the surface of SiO_2 nanoparticle through the reaction between hydroxyl groups of nanoparticle and methoxyl groups of B-TMOS during the mixing process.

The chemical structure of separated SiO_2 nanoparticles was investigated by solid-state ^{29}Si NMR spectroscopy because this technique allowed the identification of different types of silicon environments. This relies on the sensitivity of the isotropic chemical shift (δ_{iso}) for ^{29}Si towards the number of silicon–oxygen bridges and its substituents, giving rise to distinct regions for (poly)siloxanes and silicates, that is, mono-functional (M) siloxanes resonate between $\delta = 13$ and 1 ppm, difunctional (D^n) between $\delta = -7$ and -20 ppm, trifunctional (T^n) between $\delta = -49$ and -66 ppm, and tetrafunctional (Q^n) silyloxy species between $\delta = -91$ and -110 ppm. The superscript corresponds to the number of oxygen bridges to other silicon atoms [32–35]. Fig. 4 displays resulting spectrum of separated SiO_2 nanoparticles. The peaks at -42.03, -49.79 and -58.96 ppm in the spectrum were assigned to uncondensed monomer T^0, mono-substituted T^1, and disubstituted T^2 species of B-TMOS, respectively , which were in good agreement with literature values [34,36]. Consistent with FTIR, it was evident that the active methoxyl groups of B-TMOS monomer could easily react with hydroxyl groups of nanoparticles through covalent bond in B-TMOS/SiO_2 solution. It could also be seen from the spectrum that the mono-substituted B-TMOS was dominant, which was in good agreement with Yan's research [22]. The chemical structure of possible silyloxy species in separated SiO_2 nanoparticles is shown in Fig. 5. Base on relatively higher intensity of T^n compare to Q^n, we could also conclude that one SiO_2 nanoparticle could link with many B-MTOS molecules through Si–O–Si bond. Therefore, many SiO_2 nanoparticles can gather together through benzoxazine molecular and bond to PB-TMOS network tightly when oxazine ring-opening polymerization occurred, which also contributed to the surface modification in Fig. 2. The strong interaction between two phases in the PBS coating must undoubtedly be attributed to improve its barrier ability.

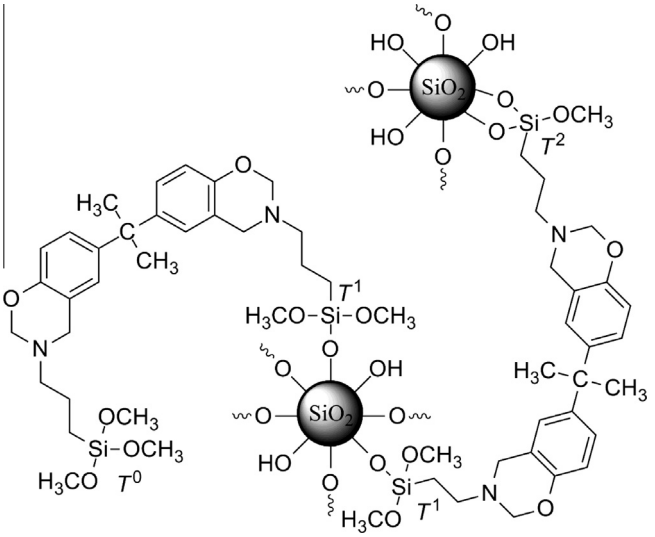

Fig. 5. Chemical structures of the possible silyloxy species in separated SiO_2 nanoparticles.

3.3. Corrosion resistance of PBS coatings

The corrosion resistance of the prepared coatings in 3.5 wt% NaCl aqueous solutions was evaluated by the open-circuit potentials (E_{ocp}), potentiodynamic polarization curves and EIS approaches. The E_{ocp} recorded for bare and coated MS are plotted as a function of immersion time, shown in Fig. 6. The E_{ocp} values corresponding to the coated samples shifted significantly in the anodic direction, from the original value of about -0.7 V (Ag/AgCl) to a value higher than -0.5 V (Ag/AgCl), and this tendency of shift to nobler potentials was also observed for the samples with SiO_2 nanoparticles. Furthermore, the E_{ocp} value of PBS coated electrodes decreased much slower than pure PB-TMOS sample during 90 min exposures to a corrosive environment. High E_{ocp} values typically indicate high corrosion resistance of coatings [37]. The increased E_{ocp} suggested that PBS coatings were less porous with a lower permeability against diffusing corrosive species [38,39], significantly enhancing barrier properties by incorporating SiO_2 nanoparticles.

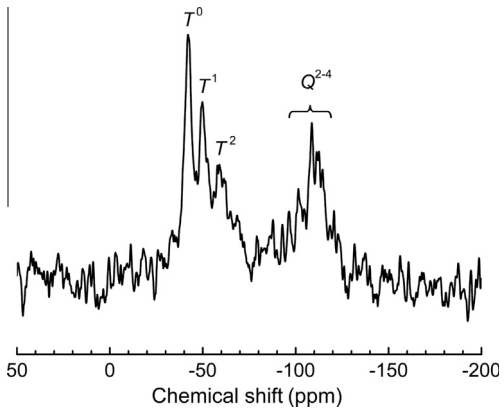

Fig. 4. Solid-state ^{29}Si NMR spectrum of separated SiO_2 nanoparticle.

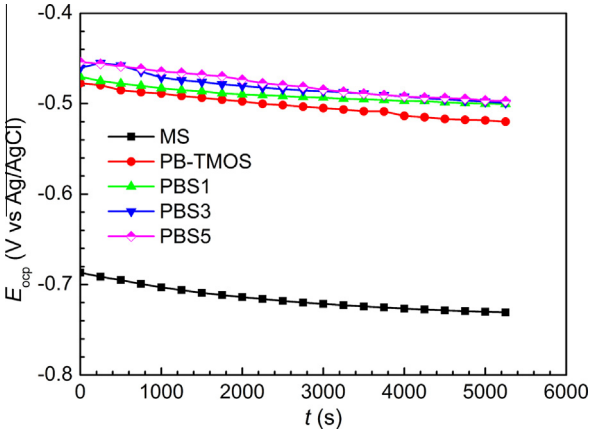

Fig. 6. E_{ocp}–time curves for different electrodes in 3.5 wt% NaCl aqueous solutions.

The number of free volumes inside the coating matrix might significantly decrease, because the cavities and holes among polymer molecules could be occupied by nanoparticles. When the content of SiO_2 nanoparticles was high (3 wt% and 5 wt%), small fluctuations in E_{ocp} values o were observed in Fig. 6 at the initial immersion times. However, the E_{ocp}/time behavior stabilized and tended to be consistent with the PBS1 sample for immersion times beyond about 1 h. The final E_{ocp} values of PBS samples were nearly the same, which was about −500 mV (Ag/AgCl). It is hard to characterize the performance of PBS samples by E_{ocp}–time curves. Therefore, the corrosion resistance of PBS samples would be investigated in detail by polarization technique and EIS technique.

Fig. 7 showed the Tafel plots of bare metal and coated samples. Curve a represented the uncoated MS, while curves b–e were for the PB-TMOS coated MS panels unloaded or loaded with different amounts of SiO_2 nanoparticles. It was found that both anodic and cathodic current densities reduced appreciably by at least one decade after coated. These decreases in current showed that the coatings inhibited both the cathodic and anodic reactions. Moreover, the anodic current corresponding to the sample with SiO_2 nanoparticles decreased more strongly than the cathodic current compared with neat PB-TMOS sample. This difference between the reduction of anodic and cathodic current could be clearly observed especially when the content of nanoparticles was low (1 wt%). It indicated that the incorporation of SiO_2 nanoparticles altered the anodic kinetics on the metal surface, and the PBS coating can inhibit the anodic reactions as a protective coating and keep the metal in a more stable state [40,41].

Fig. 8 depicts E_{corr} and corrosion rates (*CR*) of PBS coatings containing different amounts of SiO_2 nanoparticles. The corrosion potential E_{corr} and corrosion current density I_{corr} of different samples could be obtained by the Tafel extrapolation method from Fig. 7 [42]. The corrosion rate (*CR*) was calculated using the I_{corr} values and Eq. (1) [43]:

$$CR = \frac{MI_{corr}}{\rho nF} \tag{1}$$

Here I_{corr} is the corrosion density (A cm^2), M is the molecular mass of copper (58.69 g mol^{-1}), F is Faradays constant (96500 A s mol^{-1}), the material density ρ = 7.85 g cm^{-3} for MS, and the number of electrons was assumed to be 2.

The E_{corr} of the PB-TMOS/SiO_2 samples increased positively with increasing the SiO_2 nanoparticles content from about −500 mV to −480 mV (Ag/AgCl). The positive shift in E_{corr} also indicated that the incorporation of SiO_2 nanoparticles suppressed the anodic reactions on the MS surface, and therefore inhibited the entire corrosion process in the system [44]. A slight drop in *CR* value was observed corresponding to the sample with low (1 wt%) SiO_2

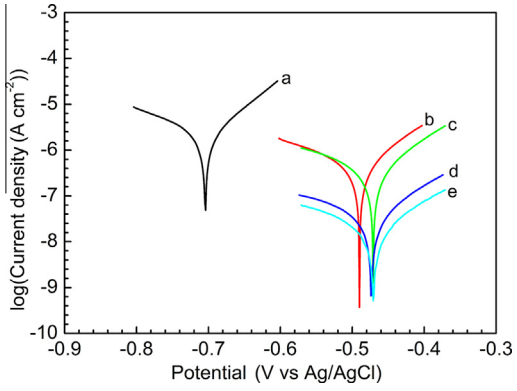

Fig. 7. Tafel curves of (a) bare MS and PB-TMOS with (b) 0 wt%, (c) 1 wt%, (d) 3 wt%, (e) 5 wt% SiO_2 nanoparticles coated MS electrodes measured in 3.5% NaCl aqueous solutions.

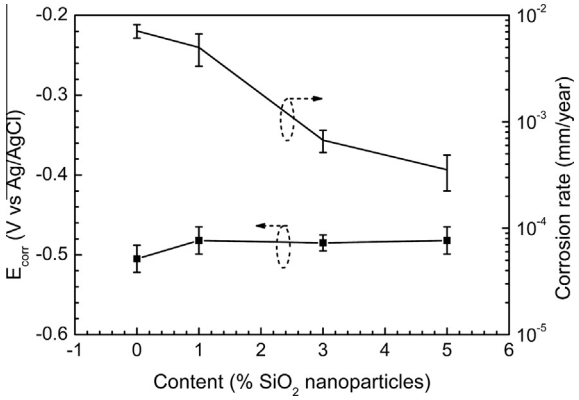

Fig. 8. The values of E_{corr} and corrosion rates (*CR*) of PB-TMOS/SiO_2 composite coatings coated MS systems are plotted as a function of the contents of SiO_2 nanoparticles.

nanoparticles content at first, as showed in Fig. 8, inferring that corrosion resistance of PB-TMOS coating was improved by incorporation of SiO_2 nanoparticles. With increasing in SiO_2 content, much higher corrosion protection ability was obtained. The *CR* value of the PB-TMOS coated sample with 3 wt% and 5 wt% SiO_2 nanoparticles was 6.73×10^{-4} mm year^{-1} and 3.55×10^{-4} mm year^{-1}, respectively, a reduction of 10 times and 15 times were observed comparing to that of the PB-TMOS coated sample without SiO_2 nanoparticles under the same conditions.

EIS Nyquist and Bode plots for different samples measured in 3.5 wt% NaCl solutions are shown in Fig. 9. As showed in both figures, the Nyquist diagrams derived from the EIS measurements featured a typical single-capacitive semi-circle, which represents the electrochemical process with only one time constant [41]. Therefore, the fitting of all EIS data was performed using a simple equivalent electric circuit model (shown in Fig. 9a), which is typically used for bare and coated MS [11]. This model includes the following elements: a resistor R_s related to resistance of the solution, a resistor R_{ct} and a capacitance C_{dl} is the resistance and capacitance of coating (the coating-electrolyte interface inside the coating), respectively. R_s is the solution resistance between the reference electrode and the working electrode (PBS coated steel), which depends not only on the resistivity of electrolyte (ionic concentration, type of ions, temperature and so on) but also on the geometry of the area in which current is carried. R_s is not a property of the coating. Therefore, it is not technically or theoretically important in the analysis of coating performance [2]. In our work, the constant phase element (*CPE*) was used to model the capacitance of the electrical double layer at the metal/liquid interface in the equivalent circuits instead of the ideal electrical capacitance. This element better describes behavior of the coatings having heterogeneities of the mesostructure and/or of the chemical composition. We translated this *CPE* information [45] (Impedance: $Z_{CPE} = 1/Q\ (i\omega)^{\alpha}$ with i is an imaginary unit, ω is an angular frequency ($\omega = 2\pi f$), α and Q is an exponential coefficient and a frequency-independent constant, respectively) into an equivalent capacitance of C_{dl}. R_{ct} is the charge transfer resistance between the metal and the liquid (metal corrosion) [46]. The calculated values of different parameters for coatings are presented in Table 2. From Fig. 9b and c, it is suggested that a good superposition with the experimental data is observed by fitting EIS data with the model, and the uncertainty of parameters in Table 2 is less than 4%, which demonstrated the reliability of fitting results. The incorporation of nanoparticles increased the charge transfer resistance R_{ct} while decreased the double layer capacitance C_{dl}, indicating reduced coating porosity and improved barrier performance for corrosion protection of the steel substrate [2,44]. A similar trend with Tafel plots and E_{ocp}–time

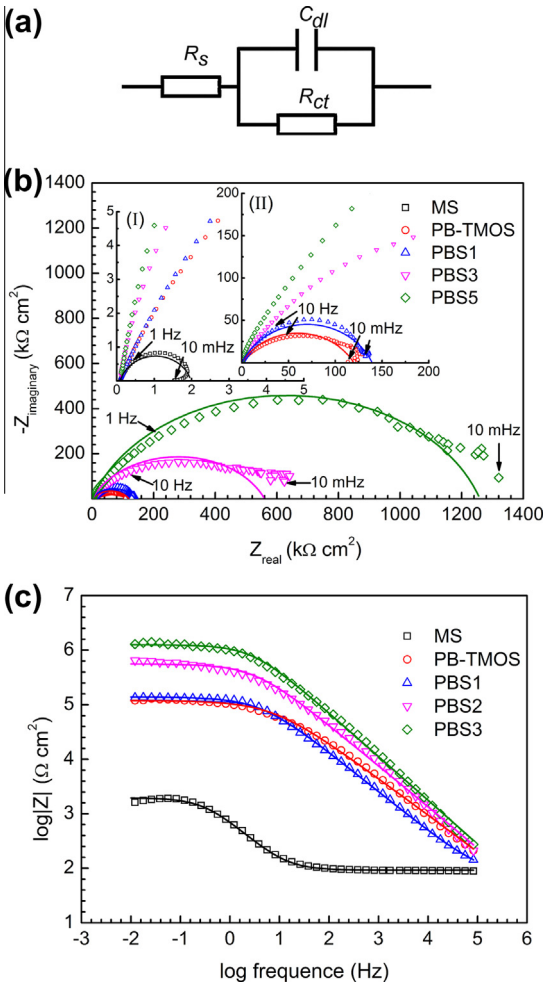

Fig. 9. (a) Equivalent circuit model used in modeling, and EIS (b) Nyquist (Inset I, II: Magnification of Nyquist plots) and (c) Bode plots for different electrodes measured in 3.5 wt% NaCl aqueous solution. Best fits to the equivalent circuit models are solid lines.

Table 2
Parameters of the equivalent circuit in 3.5 wt% NaCl solutions.

Samples	R_s (Ω cm^2)	R_{ct} (kΩ cm^2)	C_{dl} (CPE)	
			Q (Ω^{-1} cm^{-2} s$^{\alpha}$)	α
MS	94.3	1.88	2.00×10^{-3}	0.84
PB-TMOS		113.94	3.38×10^{-6}	0.58
PBS1		121.47	2.88×10^{-6}	0.67
PBS3		687.08	1.87×10^{-7}	0.75
PBS5		985.81	1.22×10^{-7}	0.80

curves was observed here, the sample, with the highest content of SiO_2 nanoparticles, had the greatest corrosion protection performance. R_{ct} increased by ~9 times and C_{dl} reduced by 27 times for the PBS5 sample compare to neat PB-TMOS sample.

3.4. Role of nanoparticles in enhancing the corrosion resistance of PBS coating

On the basis of electrochemical measurement, the PB-TMOS on loading with SiO_2 nanoparticles tended to improve the corrosion performance up to a certain extent. Two effects of nanoparticles contributed to the enhanced corrosion protection of the PB-TMOS coatings by incorporating SiO_2 nanoparticles.

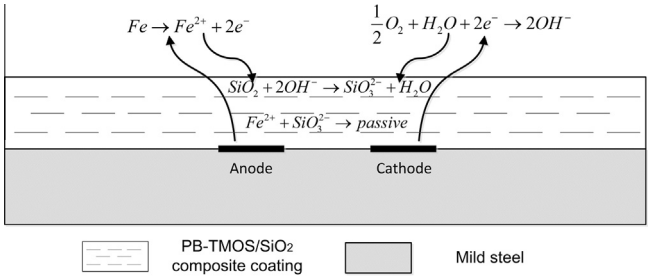

Fig. 10. Anodic protection of PB-TMOS/SiO_2 composite coatings.

3.5. Physical barrier effect

Corrosion protection of the silica-containing PB-TMOS coatings on MS was mainly brought about by the barrier effects, which could prevent oxygen and moisture from reaching the metal substrate. Hydrophobic properties of the coatings were measured by water contact angle and the results indicated that all PB-TMOS/SiO_2 coated samples were hydrophobic. It could effectively decrease wettability of the aggressive electrolyte and then limit the sorption of water at the coatings' surface. The presence of SiO_2 nanoparticles in the PBS coatings, which could bind tightly to PB-TMOS network through the cross-linking reaction between two phases, would further enhance the hydrophobicity by increasing the roughness of the PBS coating. Although nanoparticles did not distribute well due to the formation of aggregates in our system, no microcracks like literature [2] formed beside the aggregates in the coating matrix. It should ascribe to the strong interaction between two phases by the reaction of PB-TMOS and SiO_2 nanoparticles, which connected two phases tightly with the cross-linking network. The fine particles embedded in coatings also could reduce porosity of the coatings and constitute a solid barrier in the path of oxygen and water molecules passing through the coatings, retarding the progress of the penetration of aggressive species. Therefore, good barrier properties were obtained, which had been evidenced by low corrosion rates and high impedances from electrochemical measurements.

3.6. Anodic protection

Tafel polarization behavior (Fig. 7) of PBS coating showed that the anodic current decreased more strongly than the cathodic current and a positive shift in E_{corr} was also observed. It should be credited to the anodic protection effect of nanoparticles. W. J. van Ooij et al. discovered that free SiO_2 nanoparticles in coatings could react with the cathodically generated OH^- ions, and the formed SiO_3^{2-} ions can react with metal ions to form a passive silicate film [47]. As showed in Fig. 10, this passive silicate film could cover the active sites at anode and cathode in our system. So both the cathodic and anodic reactions were inhibited with the reduction of the cathodic and anodic currents simultaneously, and the suppression of the anodic reaction was more effective.

4. Conclusion

In this paper, a series of hybrid materials consisted of PB-TMOS and SiO_2 nanoparticles had been successfully prepared by a dip-coating and thermal curing technique. Results of FTIR and solid-state ^{29}Si NMR measurements verified that the SiO_2 nanoparticles had been covalent bonding with PB-TMOS, which could enhance the adhesion of SiO_2 nanoparticles in PB-TMOS matrix. Corrosion protection for the PB-TMOS coatings with different SiO_2 nanoparticles content had been evaluated by electrochemical measurements. It was found that incorporation of SiO_2 nanoparticles into the PB-TMOS coating showed a remarkable improvement in corro-

sion resistance of mild steel in 3.5 wt% NaCl solutions. Role of nanoparticles in enhancing the corrosion resistance of PBS coating should be attributed to the synergistic effect of barrier property induced from SiO_2 nanoparticles in its matrix and anodic inhibition induced from passive Fe–silicate compounds. The synergistic effects made the corrosion resistance of PBS coatings was improved with the increase of the SiO_2 nanoparticles content at the range of 1–5%, which was much better than bare MS and neat PB-TMOS coated sample.

Acknowledgements

This research was financially supported by the Nanotech Foundation of Science and Technology Commission of Shanghai Municipality (No. 0652nm001), the Fundamental Research Funds for the Central Universities, the National Natural Science Funds of China (Grant No. u1162110), Program of Shanghai Subject Chief Scientist (10XD1401500) and Lanpec Technologies Co, Ltd. The authors would like to thank to Prof. Chunzhong Li (East China University of Science and Technology) for his valuable helps with providing the SiO_2 nanoparticles utilized in this paper.

References

[1] F. Chen, P. Liu, Conducting polyaniline nanoparticles and their dispersion for waterborne corrosion protection coatings, ACS Appl. Mater. Interfaces 3 (2011) 2694–2702.
[2] X. Shi, T.A. Nguyen, Z. Suo, Y. Liu, R. Avci, Effect of nanoparticles on the anticorrosion and mechanical properties of epoxy coating, Surf. Coat. Technol. 204 (2009) 237–245.
[3] H. Shi, F. Liu, L. Yang, E. Han, Characterization of protective performance of epoxy reinforced with nanometer-sized TiO_2 and SiO_2, Prog. Org. Coat. 62 (2008) 359–368.
[4] G.P. Bierwagen, Reflections on corrosion control by organic coatings, Prog. Org. Coat. 28 (1996) 43–48.
[5] M.M. Popović, B.N. Grgur, V.B. Mišković-Stanković, Corrosion studies on electrochemically deposited PANI and PANI/epoxy coatings on mild steel in acid sulfate solution, Prog. Org. Coat. 52 (2005) 359–365.
[6] L. Liu, J.-M. Hu, W.-H. Leng, J.-Q. Zhang, C.-N. Cao, Novel bis-silane/TiO_2 bifunctional hybrid films for metal corrosion protection both under ultraviolet irradiation and in the dark, Scripta Mater. 57 (2007) 549–552.
[7] G.X. Shen, Y.C. Chen, C.J. Lin, Corrosion protection of 316 L stainless steel by a TiO_2 nanoparticle coating prepared by sol–gel method, Thin Solid Films 489 (2005) 130–136.
[8] M.M. Jalili, S. Moradian, H. Dastmalchian, A. Karbasi, Investigating the variations in properties of 2-pack polyurethane clear coat through separate incorporation of hydrophilic and hydrophobic nano-silica, Prog. Org. Coat. 59 (2007) 81–87.
[9] L.H. Yang, F.C. Liu, E.H. Han, Effects of P/B on the properties of anticorrosive coatings with different particle size, Prog. Org. Coat. 53 (2005) 91–98.
[10] B. Ramezanzadeh, M.M. Attar, An evaluation of the corrosion resistance and adhesion properties of an epoxy-nanocomposite on a hot-dip galvanized steel (HDG) treated by different kinds of conversion coatings, Surf. Coat. Technol. 205 (2011) 4649–4657.
[11] M. Behzadnasab, S.M. Mirabedini, K. Kabiri, S. Jamali, Corrosion performance of epoxy coatings containing silane treated ZrO_2 nanoparticles on mild steel in 3.5% NaCl solution, Corros. Sci. 53 (2011) 89–98.
[12] S.K. Dhoke, A.S. Khanna, Effect of nano-Fe_2O_3 particles on the corrosion behavior of alkyd based waterborne coatings, Corros. Sci. 51 (2009) 6–20.
[13] F. Dolatzadeh, S. Moradian, M.M. Jalili, Influence of various surface treated silica nanoparticles on the electrochemical properties of SiO_2/polyurethane nanocoatings, Corros. Sci. 53 (2011) 4248–4257.
[14] E. Barna, B. Bommer, J. Kürsteiner, A. Vital, O.v. Trzebiatowski, W. Koch, B. Schmid, T. Graule, Innovative, scratch proof nanocomposites for clear coatings, Compos. Part A: Appl. Sci. Manuf. 36 (2005) 473–480.
[15] H. Ishida, D.J. Allen, Physical and mechanical characterization of near-zero shrinkage polybenzoxazines, J. Polym. Sci. Part B: Polym. Phys. 34 (1996) 1019–1030.
[16] H. Dong, Z. Xin, X. Lu, Y. Lv, Effect of N-substituents on the surface characteristics and hydrogen bonding network of polybenzoxazines, Polymer 52 (2011) 1092–1101.
[17] L. Qu, Z. Xin, Preparation and surface properties of novel low surface free energy fluorinated silane-functional polybenzoxazine films, Langmuir 27 (2011) 8365–8370.
[18] H. Ishida, H.Y. Low, A study on the volumetric expansion of benzoxazine-based phenolic resin, Macromolecules 30 (1997) 1099–1106.
[19] H.-C. Liu, W.-C. Su, Y.-L. Liu, Self-assembled benzoxazine-bridged polysilsesquioxanes exhibiting ultralow-dielectric constants and yellow-light photoluminescent emission, J. Mater. Chem. 21 (2011) 7182–7187.
[20] M.-C. Tseng, Y.-L. Liu, Preparation, morphology, and ultra-low dielectric constants of benzoxazine-based polymers/polyhedral oligomeric silsesquioxane (POSS) nanocomposites, Polymer 51 (2010) 5567–5575.
[21] C. Zhou, X. Lu, Z. Xin, J. Liu, Corrosion resistance of novel silane-functional polybenzoxazine coating on steel, Corros. Sci. 70 (2013) 145–151.
[22] C. Yan, X. Fan, J. Li, S. Zhiqi Shen, Study of surface-functionalized nano-SiO_2/polybenzoxazine composites, J. Appl. Polym. Sci. 120 (2011) 1525–1532.
[23] L. Zhang, Y. Hong, T. Zhang, C. Li, A novel approach to prepare PBT nanocomposites with elastomer-modified SiO_2 particles, Polym. Compos. 30 (2009) 673–679.
[24] H.J. Lee, S. Michielsen, Preparation of a superhydrophobic rough surface, J. Polym. Sci. Part B: Polym. Phys. 45 (2007) 253–261.
[25] C.-F. Wang, Y.-T. Wang, P.-H. Tung, S.-W. Kuo, C.-H. Lin, Y.-C. Sheen, F.-C. Chang, Stable superhydrophobic polybenzoxazine surfaces over a wide pH range, Langmuir 22 (2006) 8289–8292.
[26] L.B. Boinovich, S.V. Gnedenkov, D.A. Alpysbaeva, V.S. Egorkin, A.M. Emelyanenko, S.L. Sinebryukhov, A.K. Zaretskaya, Corrosion resistance of composite coatings on low-carbon steel containing hydrophobic and superhydrophobic layers in combination with oxide sublayers, Corros. Sci. 55 (2012) 238–245.
[27] L. Boinovich, A. Emelyanenko, A wetting experiment as a tool to study the physicochemical processes accompanying the contact of hydrophobic and superhydrophobic materials with aqueous media, Adv. Colloid Interf. Sci. 179–182 (2012) 133–141.
[28] J. Dunkers, H. Ishida, Vibrational assignments of N,N-bis(3,5-dimethyl-2-hydroxybenzyl)methylamine in the fingerprint region, Spectrochim. Acta Part A: Mol. Biomol. Spectroscop. 51 (1995) 855–867.
[29] Y. Liu, Z. Yue, J. Gao, Synthesis, characterization, and thermally activated polymerization behavior of bisphenol-S/aniline based benzoxazine, Polymer 51 (2010) 3722–3729.
[30] T. Takeichi, T. Kano, T. Agag, Synthesis and thermal cure of high molecular weight polybenzoxazine precursors and the properties of the thermosets, Polymer 46 (2005) 12172–12180.
[31] T. Agag, T. Takeichi, Synthesis and characterization of benzoxazine resin-SiO_2 hybrids by sol–gel process: the role of benzoxazine-functional silane coupling agent, Polymer 52 (2011) 2757–2763.
[32] R. Joseph, S. Zhang, W.T. Ford, Structure and dynamics of a colloidal silica–poly(methyl methacrylate) composite by 13C and ^{29}Si MAS NMR spectroscopy, Macromolecules 29 (1996) 1305–1312.
[33] Y. Liu, W. Zhang, Y. Chen, S. Zheng, Polybenzoxazine containing polysilsesquioxane: preparation and thermal properties, J. Appl. Polym. Sci. 99 (2006) 927–936.
[34] X. Lu, Q. Yin, Z. Xin, Z. Zhang, Powerful adsorption of silver(I) onto thiol-functionalized polysilsesquioxane microspheres, Chem. Eng. Sci. 65 (2010) 6471–6477.
[35] A.K.W. Lippach, R. Krämer, M.R. Hansen, S. Roos, K. Stöwe, M. Stommel, G. Wenz, W.F. Maier, Synthesis and mechanical properties of organic–inorganic hybrid materials from lignin and polysiloxanes, ChemSusChem 5 (2012) 1778–1786.
[36] C.R. Miller, R. Vogel, P.P.T. Surawski, K.S. Jack, S.R. Corrie, M. Trau, Functionalized organosilica microspheres via a novel emulsion-based route, Langmuir 21 (2005) 9733–9740.
[37] S. Radhakrishnan, C.R. Siju, D. Mahanta, S. Patil, G. Madras, Conducting polyaniline–nano-TiO2 composites for smart corrosion resistant coatings, Electrochim. Acta 54 (2009) 1249–1254.
[38] B. Nikravesh, B. Ramezanzadeh, A.A. Sarabi, S.M. Kasiriha, Evaluation of the corrosion resistance of an epoxy-polyamide coating containing different ratios of micaceous iron oxide/Al pigments, Corros. Sci. 53 (2011) 1592–1603.
[39] T. Tüken, A.T. Özyılmaz, B. Yazıcı, M. Erbil, Electrochemical synthesis of polyaniline on mild steel in acetonitrile–$LiClO_4$ and corrosion performance, Appl. Surf. Sci. 236 (2004) 292–305.
[40] D.-Q. Zhang, L.-X. Gao, G.-D. Zhou, Self-assembled urea-amine compound as vapor phase corrosion inhibitor for mild steel, Surf. Coat. Technol. 204 (2010) 1646–1650.
[41] T.-C. Huang, Y.-A. Su, T.-C. Yeh, H.-Y. Huang, C.-P. Wu, K.-Y. Huang, Y.-C. Chou, J.-M. Yeh, Y. Wei, Advanced anticorrosive coatings prepared from electroactive epoxy–SiO_2 hybrid nanocomposite materials, Electrochim. Acta 56 (2011) 6142–6149.
[42] W.-G. Ji, J.-M. Hu, J.-Q. Zhang, C.-N. Cao, Reducing the water absorption in epoxy coatings by silane monomer incorporation, Corros. Sci. 48 (2006) 3731–3739.
[43] X. Zhang, W. He, I. Wallinder, J. Pan, C. Leygraf, Determination of instantaneous corrosion rates and runoff rates of copper from naturally patinated copper during continuous rain events, Corros. Sci. 44 (2002) 2131–2151.
[44] H. Yun, J. Li, H.-B. Chen, C.-J. Lin, A study on the N-, S- and Cl-modified nano-TiO2 coatings for corrosion protection of stainless steel, Electrochim. Acta 52 (2007) 6679–6685.
[45] P. Córdoba-Torres, T.J. Mesquita, R.P. Nogueira, Toward a better characterization of constant-phase element behavior on disk electrodes from direct impedance analysis: methodological considerations and mass transport effects, Electrochim. Acta 92 (2013) 323–334.
[46] D. Prasai, J.C. Tuberquia, R.R. Harl, G.K. Jennings, K.I. Bolotin, Graphene: corrosion-inhibiting coating, ACS Nano 6 (2012) 1102–1108.
[47] V. Palanivel, D. Zhu, W.J. van Ooij., Nanoparticle-filled silane films as chromate replacements for aluminum alloys, Prog. Organ. Coat. 47 (2003) 384–392.